ELSEVIER

Heat transfer enhancement in electronic modules using ribs and "film-cooling-like" techniques

B. A. Jubran and A. S. Al-Salaymeh
Department of Mechanical Engineering, University of Jordan, Amman, Jordan

This paper reports an experimental investigation to study the effects of using various sizes and shapes of ribs, the presence of secondary air-flow injections through cylinders and "film-cooling-like" injection holes on the heat transfer coefficient and the pressure drop characteristics of an array of rectangular modules at different values of Reynolds numbers in the range $4.0 \times 10^3 - 2.5 \times 10^4$. Generally, it was found that using different sizes and shapes of ribs as well as the presence of secondary air-flow injection cylinders and film-cooling-like injection holes tends to increase the Nusselt number by as much as 50, 46 and 43% for the rectangular, triangular, and cylindrical ribs, respectively. The film-cooling-like technique tends to give heat transfer enhancement of as much as 51%, which is about that of the rectangular ribs but with very much less pressure drop.

Keywords: heat-transfer enhancement; film cooling

1. Introduction

Cooling of electronic components continues to attract much research activity toward achieving effective cooling techniques to meet the design and the development of rather complex circuits and highly dense electronic boards, characterized by high rate of heat dissipation per unit of components area. The topography of the electronic board plays a significant role in the heat transfer rate and the pressure drop characteristics of these boards.

Sparrow et al. (1982,1983) reported data for heat transfer and pressure drop for airflows in arrays of heat-generating square modules located along one wall of a flat rectangular duct. The effects of missing modules as well as the implantation of barriers at various locations were investigated. It was found that an increase in heat transfer coefficient of as much as 40% is obtained when the missing module is located upstream of the module of interest. The use of barriers in the array was found to be effective in enhancing the heat transfer coefficient by a maximum factor of two. Torikoshi et al. (1988) reported the heat transfer characteristics of arrays of modules with sudden change in their heights. It was found that for the fully populated arrays, the per block Nusselt number decreased monotonically with increasing distance in the streamwise direction. On the other hand, the per block Nusselt number was increased in the streamwise direction when there are abrupt changes in the heights of the modules.

Buller and Kilburn (1981) investigated the convective heat transfer from single-rectangular modules. Five specimens were tested: three plain square modules and two square modules with finned heat sinks attached. A single correlation based on the Reynolds number and Nusselt number was obtained and found to fit the results within 15% for all five modules. Wirtz and Dykshoorn (1984) investigated heat transfer coefficient from square modules, each of 2.54×2.54 cm^2 and 0.635 cm in height. The elements were implanted in a sparse array with gaps of 2.54 cm between the adjacent elements, in both the streamwise and spanwise directions.

Moffat et al. (1985) described an experimental study of forced-convection related to the thermal protection of individual elements in an air-cooled array of electronic components. Heat transfer coefficient results and thermal wake function were presented for in-line arrays of cubical elements. Ratts et al. (1988) presented an experimental study of internal flow modulation induced by vortex shedding from cylinder in cross-flow and its effect on cooling an array of chips. They concluded that a heat transfer coefficient increase of up to 82% can be obtained when cylinders are placed periodically above the back edge of each row of chips. Myrum et al. (1993) investigated the heat transfer and the pressure characteristics of airflow in a ribbed duct with vortex generator placed immediately upstream or just downstream of selected rib elements. Provided the diameter of the generator is large, the average Nusselt number was increased by as much as 21%.

Molki et al. (1994) conducted an experimental investigation to study the pressure drop in the entrance region of an array of rectangular modules fixed to the bottom duct wall. They used flow visualization and found a highly separated region on the first module of the array.

Lau et al. (1989) studied the effects of lateral flow ejection on the overall heat transfer coefficient and pressure drops for turbulent flow through pin fin channels and found that the Nusselt number has increased with increasing the Reynolds number and is reduced by as much as 25% as the ejection ratio is increased

Address reprint requests to Prof. B. A. Jubran, Faculty of Engineering and Technology, University of Jordan, Amman, Jordan.

Received 22 June 1995; accepted 26 October 1995

Int. J. Heat and Fluid Flow 17: 148–154, 1996

655 Avenue of the Americas, New York, NY 10010

0142-727X/96/$15.00
SSDI 0142-727X(95)00098-4

from 0 to 1.0. Lehmann and Huang (1991) investigated the potential of using a secondary flow mixing to enhance convective air cooling of board-mounted electronic components through the the use of vortex generators.

The aim of the present investigation is to study the heat transfer and the pressure drop characteristics for a uniform array of blocks in the presence of ribs of different shapes. Furthermore, a technique similar to the well-established technique of film cooling used in the cooling of gas turbine blades is investigated with reference to cooling of electronic modules.

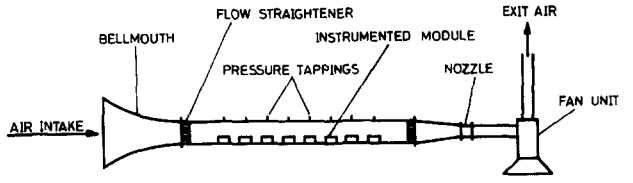

Figure 1 General layout of the experimental setup.

Experimental rig and experimentation

The experimental setup used in this investigation is basically a modified version of that used by Hollworth and Durbin (1992). The setup consists mainly of a suction-type wind tunnel with maximum flow rate of 0.24 m^3/s. The main body of the test section is a channel-like box 2-m in length, 0.33-m in width, and 0.04-m in height.

The test section and the wind tunnel have been constructed from 3-mm sheet metal. The front sidewall of the test section accommodates at its middle section a double glazed window to ease observation of the array configurations during tests. At the air intake side of the wind tunnel, a bellmouth is attached, and a flow straightener is placed at the front as well as at the trailing edge of the wind-tunnel test section with a gradual contraction connected to a circular cross-section pipe of the fan (Figure 1).

The modules array consists of uniform individual rectangular elements manufactured from light metal aluminium alloy duralumin. The modules in the array are arranged in eight rows each containing five elements. The basic dimensions of the modules are 25-mm side length, 15-mm width, and 10-mm height. It should be pointed out that the long side of the module is always parallel to the airflow. The spacings between the modules are 25 mm and 15 mm, in the streamwise and spanwise directions, respectively. Figure 2a shows a typical basic array configuration in the test section.

Three different shapes and sizes of ribs were used and fixed to the array board; namely, rectangular, triangular, and cylindrical ribs. The ribs were manufactured from balsa with two basic dimensions for each shape giving six basic dimension ribs altogether. The length of all of these ribs are the same and equal to the width of the board, while the height and the width of these ribs are equal. The heights of the various ribs used are 8 mm and 16 mm. The height of the ribs in Figure 2b can be specified in dimensionless form as $b/t = 0.8$ and 1.6, where t is the height of the modules. The ribs have been inserted in the fully developed region in the gap between the fifth and the sixth row, as shown in Figure 2b,c.

The secondary flow injection and the film-cooling-like techniques were carried out by drawing air from a fan and then feeding it to a settling chamber that accommodates the injection mechanism. The injection mechanism consists of one row of five perspex tubes of 10-mm outside diameter and 5-mm inside diameter with the distance between the injection holes given by $P/D = 6$. Two arrangements were used; the first one is that of the secondary flow injection where the five tubes were simply and independently penetrated through the board and were allowed to be flush with the modules, Figure 3a, while the second

Notation

A_c	flow cross section associated with the gap height S (m^2)
A_{surf}	modules exposed area, m^2
b	height of the rib, m
c_p	specific heat of air (kJ/kg · K)
C_p	per row pressure coefficient for nonuniform array configurations
C_{po}	per row pressure coefficient for uniform array configuration
D	diameter of the injection cylinders or holes
E	input voltage to the elements heater, V
h	heat transfer coefficient ($W/m^2 \cdot K$)
H	height of the test section channel, m
I	input current to the elements heater, A
k_{air}	thermal conductivity of air, W
L	module side length, m
M	blowing rate
N	downstream row number or total number of modules downstream of the module of interest
Nu	Nusselt number for nonuniform array configurations (hL/k_{air})
Nu_o	Nusselt number for uniform array configurations (hL/k_{air})
P	distance between the injection holes, m
q	heat flux rate, W
Re	Reynolds Number, ($\dot{w}L/A_c\nu$)
S	test-section channel height, m
t	module height, m
T_1	temperature of the first module just downstream of the active module, K
T_{act}	surface temperature of the active module, K
T_N	temperature of the module at the Nth row downstream the active module, K
T_{ref}	reference temperature of the fluid, K
U	mean velocity m/s
$\dot{w}$	air flow rate through the channel m^3/s

Greek

ν	kinematic viscosity for air, m^2/s
ρ	air density, kg/m^3
θ	thermal wake function
θ_1	thermal wake function of the first module next to the active module
θ_N	thermal wake function at the module N along the channel in the same column as the active module

Subscripts

a	air
act	active
conv	convection
i	injection
ref	reference
S	based on the channel height
∞	free stream

arrangement is the film-cooling-like, the five tubes are interconnected by a flat plate to form an injection rib box, which again is flush with the modules Figure 3b. The injection mechanisms for the two techniques are located between the fifth and sixth rows of modules. The quantities of injection air to that of free stream are quantified using the blowing rate, which is defined as $M = \rho_i U_i / \rho_\infty U_\infty$. Three blowing rates for the secondary injection were used; namely 0.1, 0.5, and 1; while for the film-cooling-like, the blowing rates used were 0.2, 0.5, 0.7, and 1. These experiments were conducted at a fixed free stream Reynolds number equal to 1.6×10^4.

Each of the active modules is hollowed to the same size of the heater, such as that used to accommodate a 22 Ω resistance heater, each rated at 2 W. The leads of the heaters are insulated and are connected to a variable power supply. The module's power is held constant during the experiment, so that the per module heat flux is kept constant. The modules on the array test surface are fixed to a 3-mm balsa that is fixed to a 5-mm wood sheet (Figure 4). Each module in the array is threaded to accommodate a 3-mm screw, so that the modules are well attached to the base sheet.

The steady-state temperature of the rectangular modules was obtained by embedding two copper–constantan thermocouples to the surface of each module of interest. All thermocouples were connected via the 3530 Orion-A data logger. The pressure drop across the modules arrays was determined by a total of 24 static pressure tappings mounted on the roof of the test section just

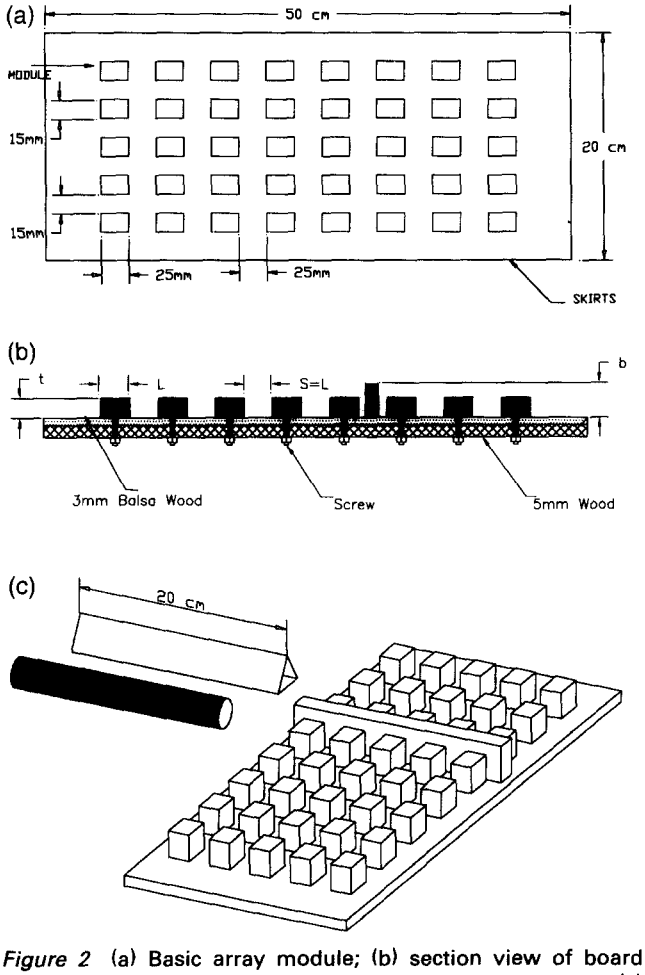

Figure 2 (a) Basic array module; (b) section view of board showing the geometrical characteristics of the array; and (c) three-dimensional (3-D) view of the board with the arrangement of ribs.

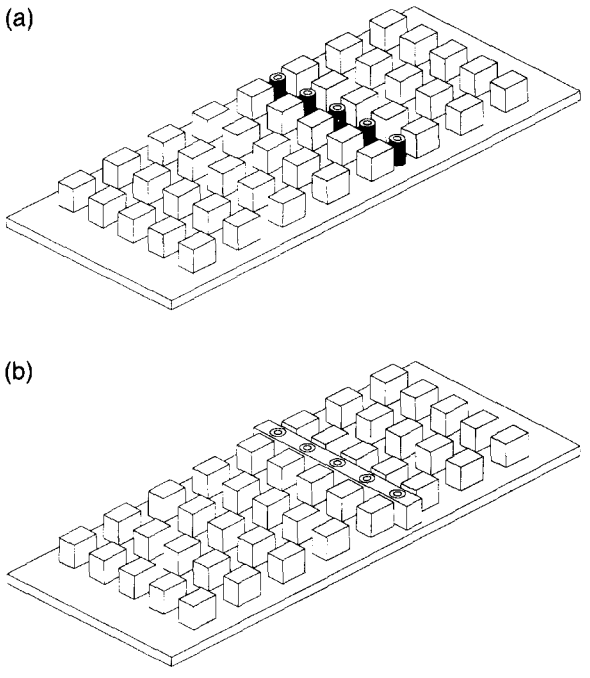

Figure 3 (a) 3-D view of the rectangular board with secondary airflow through injection tubes; (b) 3-D view of the film-cooling-like technique.

over the module array, and these were connected to an inclined manometer sensitive to the measurements of small deflections as low as 0.05 mm of ethanol. This arrangement of pressure tapping enables pressure drop to be obtained along the module array as well as at locations before and after the array. At each row there exist three tappings, and the average of these was taken as the static pressure at that location. The air-flow rate was determined using a standard nozzle of 7.02-cm in diameter with a coefficient of discharge of 0.96 installed at the inlet section of the fan. Various flow rates were obtained by varying the speed of the fan.

Once the desired array configuration was installed in the test section, the fan was switched on with the right amount of airflow. The temperature of the secondary injected air is the same as that of the main flow in the test section. The heaters were also switched on, and the experimental setup was allowed to reach steady state, which was obtained after about 1 hour. At this instant, readings of temperature, input power, pressure drop, and inlet temperature were recorded. The same procedure was repeated for different array configurations and flow rates.

Data reduction

The convective heat transfer rate q was determined from the electrical power input to the module using

$$q = EI - \Delta q \tag{1}$$

where the term Δq is a small correction for conduction and radiation heat losses from the module. To minimize the radiation losses, the modules have been polished. The conduction heat losses have been minimized by fixing the modules to the balsa plate. Hollworth and Durbin (1992) reported that the conduction losses through such a surface never exceed 4% of the heat input to the module. Furthermore, the same test surface was used by Wirtz and Dykshoorn (1984), and it was shown by thermal images technique that very little spreading of heat was conducted into the balsa surface adjacent to the heat-dissipating modules.

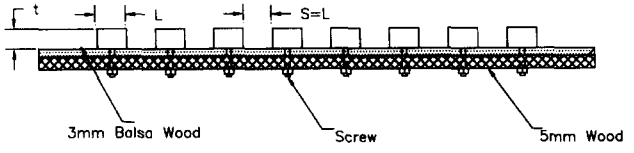

Figure 4 Front view of the module array

Assuming an emissivity of 0.12 for the module's surface, the correction factor combining both of these losses should not exceed 10% of the electrical power input.

The heat transfer coefficient was calculated from

$$h = \frac{q}{A_{\text{surf}}(T_{\text{act}} - T_{\text{ref}})} \tag{2}$$

where q is the heat input to the active module, A_{surf} represents the five surface areas of the active module exposed to the air flow, T_{act} is the active module surface temperature, and T_{ref} is the steady-state temperature of the passive modules at the first row of the array.

Thermal wake generation is experienced when an element in the array is heated. This thermal wake affects the modules downstream. The thermal wake function θ_N is defined as

$$\theta_N = \frac{T_N - T_{\text{ref}}}{T_{\text{act}} - T_{\text{ref}}} \tag{3}$$

where T_N is the temperature of the module of interest in the Nth row downstream of the active module, assuming that both of these modules are in the same column.

The temperature rise of the downstream passive module depends on the downstream distance from the active module. Taking the active module to be at $N = 0$, the dimensionless temperature rise of the first passive module downstream is expressed as

$$\theta_1 = \frac{T_1 - T_{\text{ref}}}{T_{\text{act}} - T_{\text{ref}}} \tag{4}$$

Reynolds number Re and Nusselt number Nu are calculated from:

$$\text{Re} = \frac{\dot{w}L}{A_c \nu} \tag{5}$$

$$\text{Nu} = \frac{hL}{k_{\text{air}}} \tag{6}$$

where $\dot{w}$, L, A_c, ν, and k_{air} are the air volumetric flow rate, the module side length parallel to the direction of the airflow, the cross-sectional area of the empty space over the modules, the kinematic viscosity of air, and the thermal conductivity of the air, respectively.

Presentation of the pressure drop results were classified into two groups. The first group is that for basic uniform modules array configuration where a fully developed regime is established. In this region, the per row pressure drop, Δp_{row}, is expressed in terms of the per row pressure coefficient as

$$C_{po} = \frac{\Delta p_{\text{row}}}{1/2\rho V^2} \tag{7}$$

where V is calculated as $\dot{w}/A_c$, and ρ is the air density. The second group of the pressure drop is that of the modules array configurations of different lengths, heights, and widths, where substantial increase or decrease in pressure drop occurs, and this is expressed in dimensionless form as C_p/C_{po}, where C_p represents the per row pressure drop coefficient for the nonbasic array configuration having several rows, some of which may have cylinders, different size modules, or empty spaces.

Results and discussions

Throughout the measurements made to establish the data presented in this paper, care was taken to note possible sources of error, and an error analysis based on the method of Kline and McClintock (1953) was carried out. The error analysis indicated a $\pm 3\%$ uncertainty in both the heat transfer and pressure coefficients, and $\pm 2\%$ in the velocity. Tests were repeated a few times to ensure the repeatability of the results.

Heat transfer

The row-by-row distribution of the per block Nusselt number for the basic uniform module array configuration is shown in Figure 5, for six different values of Reynolds numbers; Re = 4.0×10^3, 8.0×10^3, 1.2×10^4, 1.6×10^4, 2.0×10^4, and 2.5×10^4. These results show that for all Re values, the maximum Nu is attained at the first row of modules, which is attributed to the impingement of the flow on the first row of modules. Downstream of the first row, the Nu is decreased with the distance increase until the fourth row of modules, after which the Nu is independent of the row location. These rows are consequently considered as the fully developed region in the array. These results for the basic uniform module array configuration together with those of Sparrow et al. (1982), Torikoshi et al. (1988), Wirtz and Dykshoorn (1984), and

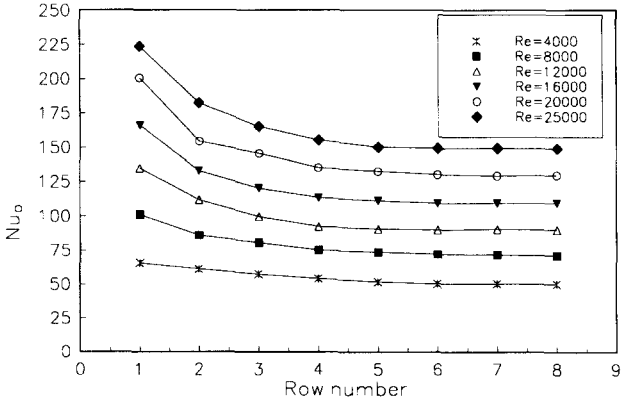

Figure 5 Row-by-row Nusselt number distributions for fully populated array.

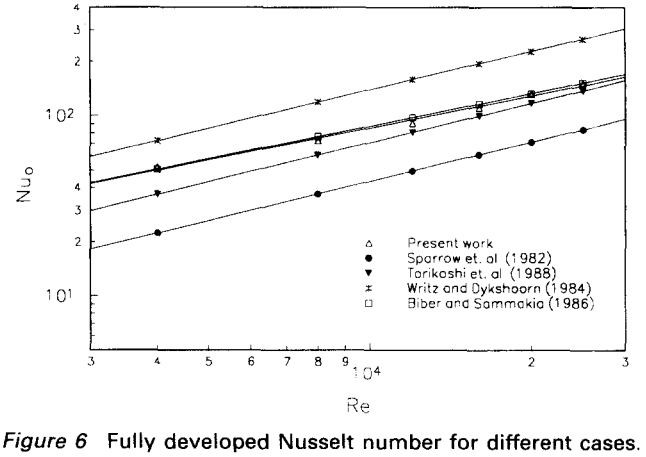

Figure 6 Fully developed Nusselt number for different cases.

Biber and Sammakia (1986) are shown in Figure 6. These results were correlated using the following form

$$\mathrm{Nu}_o = a\ \mathrm{Re}^b \tag{8}$$

where Nu_o is the average value of Nusselt number in the fully developed region of the array. It is interesting to note that the value of exponent b for all investigations that are shown in Figure 6 is more or less about 0.72. On the other hand, the values of the constant a are very much dependent on the dimensions of the modules and the other array configurations parameters. It seems that the present work is the only one that has made use of rectangular modules, while the other mentioned investigations used square ones. It can be concluded from this that when the rectangular modules are used in an array configuration, they tend to enhance the heat transfer rate over that when square modules are used. For the present investigation with $L/H = 0.625$ and the range of Re used, the following correlation was obtained

$$\mathrm{Nu}_o = 0.106\ \mathrm{Re}^{0.72} \tag{9}$$

The effects of inserting different rib heights and shapes between the fifth and sixth rows on the heat transfer characteristic of the uniform array configuration are shown in Figures 7a,b, and 8a,b. The results are plotted in terms of the ratio of Nu of the array with different rib heights, to that Nu_o of the basic array configuration with uniform modules array.

The per row distributions of $\mathrm{Nu}/\mathrm{Nu}_o$ when the ribs height ratio $b/t = 0.8$ and for two Reynolds numbers are shown in Figures 7a,b. It can be seen from these figures that at this height ratio no enhancement is observed for all Reynolds numbers investigated. However, increasing the ribs height ratio to $b/t =$ 1.6 resulted in a significant heat transfer enhancement downstream the ribs for all Reynolds numbers and shapes investigated, Figure8 a,b. The maximum enhancement in the heat transfer coefficient occurs at the seventh row and at $\mathrm{Re} = 8 \times 10^3$ with a value of 37% for the rectangular shape, 33% for the triangular shape, and 27% for the cylindrical shape.

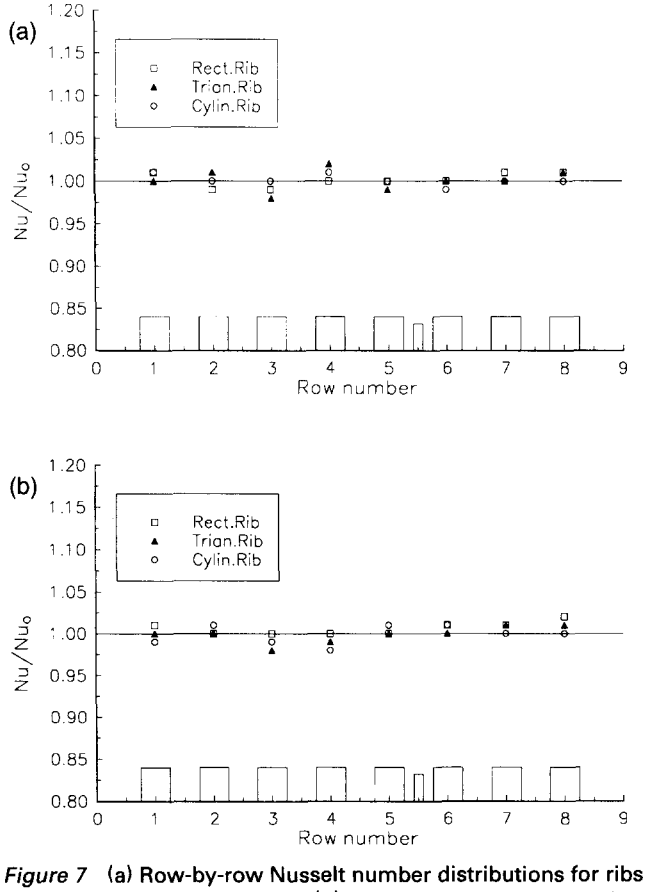

Figure 7 (a) Row-by-row Nusselt number distributions for ribs at $b/t = 0.8$ and at Re = 8000; (b) Row-by-row Nusselt number distributions for ribs at $b/t = 0.8$ and at Re = 16,000.

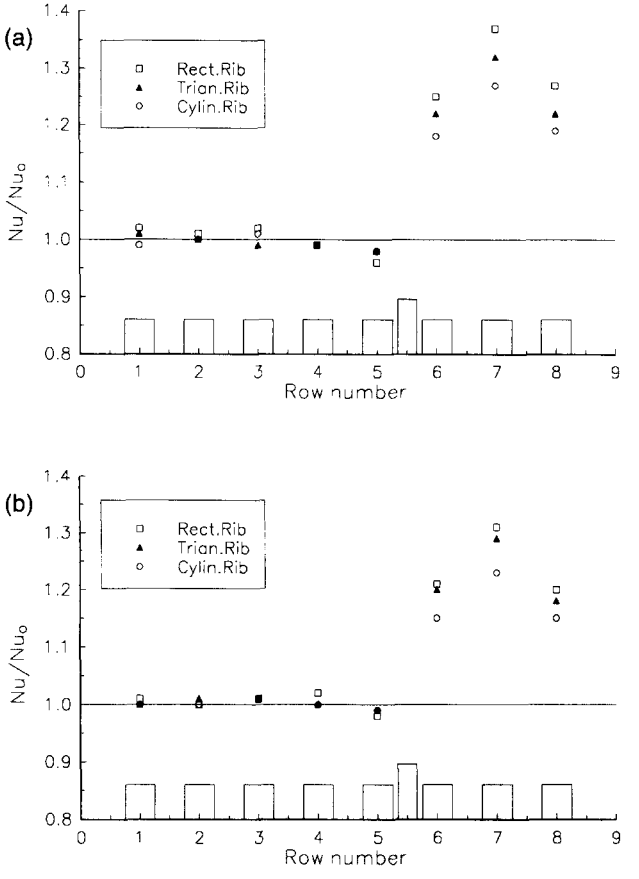

Figure 8 (a) Row-by-row Nusselt number distributions for ribs at $b/t = 1.6$ and at Re = 8000; (b) Row-by-row Nusselt number distributions for ribs at $b/t = 1.6$ and at Re = 16,000.

Although no detailed flow measurements or flow visualization have been carried out in the present investigation, we can attribute the heat enhancement in the seventh row to the changes that might have occurred in the flow structure because of change in the size of the rib, which resulted in the airflow being lifted off and then reattached at this row. The enhancement is found to be more significant at low Reynolds number, because the flow is more susceptible to disturbances than when Reynolds number is high.

The $\mathrm{Nu}/\mathrm{Nu}_o$ distributions when using secondary air-flow injection through tubes are shown in Figure 9. Three values of blowing rates at $\mathrm{Re} = 1.6 \times 10^4$ were used; 0.1, 0.5, and 1.0. It can be seen from this figure that the heat enhancement is increased with increasing blowing rate. A maximum enhancement of 40% in the heat transfer coefficient occurs at the seventh row when the blowing rate = 1. It should be pointed out that the enhancement that occurs here is caused by the tube itself being a rib, but at the same time, part of the enhancement is caused by introduction of the secondary air.

The $\mathrm{Nu}/\mathrm{Nu}_o$ distributions for the film-cooling-like at $\mathrm{Re} = 1.6 \times 10^4$ and for four blowing rates; 0.2, 0.5, 0.7, and 1.0 are shown in Figure 10. The results indicate that the enhancement in the heat transfer rate is larger than those obtained using ribs of different heights. For blowing rate $M = 1$, the Nusselt number for the row just downstream the injection holes are 42% higher than the basic array and 51% for the subsequent seventh row. For the

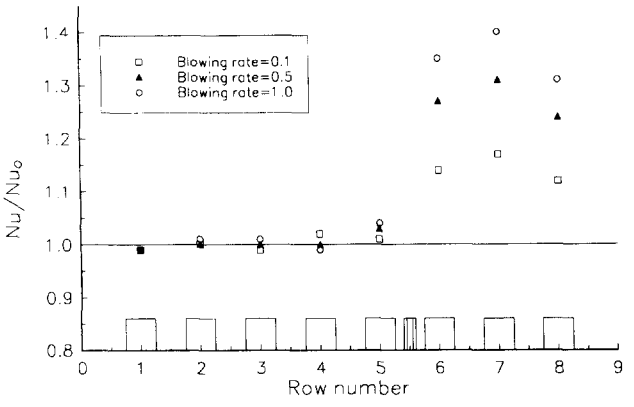

Figure 9 Row-by-row Nusselt number distributions for secondary airflow through injection tubes at Re = 16,000.

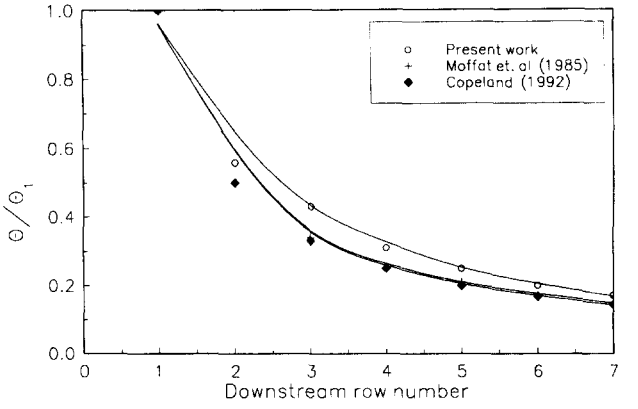

Figure 11 Dimensionless temperature distribution of the modules in the same column with the heated modules in the first row.

row just immediately upstream of the injection holes, an enhancement of 7% is achieved. This may be explained by the fact that at high blowing rate, the jets have enough momentum to lift off and then bend over to reattach at the rows further downstream from the injection holes.

The temperature distribution of the modules of the basic array along the test section in the direction of the flow was obtained by monitoring the temperature of the active module at the first row as well as the temperature of the other passive modules downstream along the same column of the active module. It should be pointed out that the effect of the thermal wakes on the flanking columns has been observed to be negligible. Figure 11 presents the dimensionless temperature distribution along the test section, at the same column of the active module and at $\mathrm{Re} = 1.6 \times 10^4$ compared with the results of Moffat et al. (1985) and Copeland (1992). It can be seen that the effect of the thermal wake is felt at the first four to five rows downstream the active module with similar trend to that observed by Moffat et al (1985) and Copeland (1992).

Pressure drop

The effect of the presence of different size and shapes and secondary air-flow injection located between the fifth and sixth rows at $8 \times 10^3 \leq \mathrm{Re} \leq 1.6 \times 10^4$ has been investigated, and the obtained results of C_p/C_{po} are shown in Figure 12a,b, where C_p is the local pressure coefficient for the arrays with different size ribs and secondary injection airflow, and C_{po} is the local pressure coefficient of the basic uniform array.

The per row pressure coefficients ratio distributions when $b/t = 0.8$, and $b/t = 1.6$, are shown in Figure 12a,b. As the height of the ribs is increased the pressure drop is increased, with the rectangular shape having the highest pressure drops at the sixth row downstream the ribs. As the flow crosses the array board and reaches just before the fifth row, no effects have been observed. However, after the fifth row, the flow pinches the top part of the rib, and this gives rise to a sharp pressure loss. The maximum pressure drop occurs at $b/t = 1.6$ and reaches a value of 70%.

The pressure coefficient ratio distributions for the secondary air-flow injection through tubes are shown in Figure 13a for three blowing rates; 0.1, 0.5, and 1.0. It can be seen from the figure that as the blowing rate is increased from 0.1 to 1.0, the channel

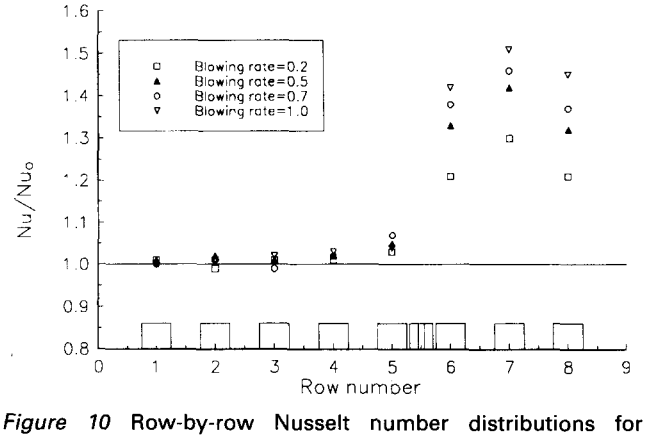

Figure 10 Row-by-row Nusselt number distributions for film-cooling-like at Re = 16,000.

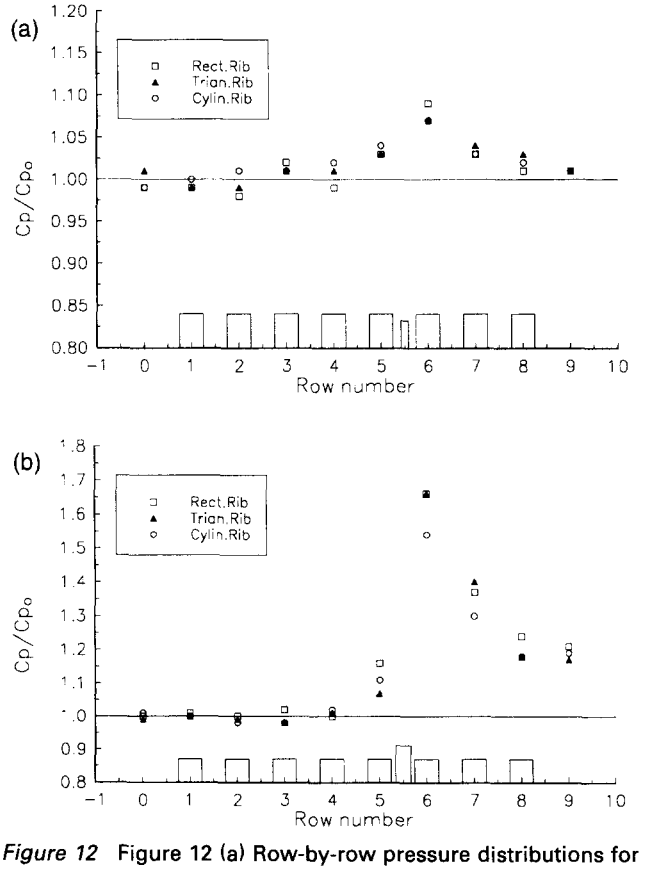

Figure 12 Figure 12 (a) Row-by-row pressure distributions for ribs at $b/t = 0.8$ and at Re = 16,000; (b) row-by-row pressure distributions for ribs at $b/t = 1.6$ and at Re = 16,000.

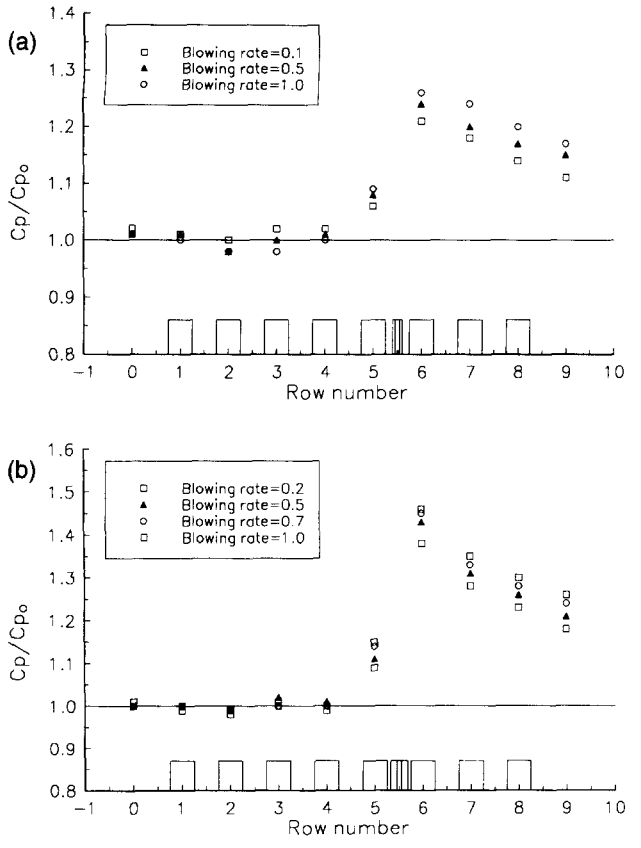

Figure 13 (a) Row-by-row pressure distributions for secondary air-flow rate through injection tubes at Re = 16,000; (b) row-by-row pressure distributions for film-cooling-like method at Re = 16,000.

flow velocity increased at a fixed mainstream Reynolds number, and the pressure losses above the array board in the channel flow is increased. The maximum pressure losses take place at the eight row with a value of 26%. This value is slightly small when compared with the results obtained for ribs.

The results of the pressure coefficient ratio distributions are shown in Figure 13b for the film-cooling-like method at a fixed Re and four blowing rates; 0.2, 0.5, 0.7, and 1.0. The mixing of the two flows increases the pressure drop coefficients. The incremental increase in the pressure drop is small and less than those obtained for the ribs. The maximum value of the pressure drop occurs at a blowing rate of 1.0 with 46% increase at the sixth row, 35% at the seventh row, and 30% for the eighth row. At is interesting to note that the pressure drop coefficient for the film-cooling-like is less than those for the array configurations with ribs of $b/t = 1.6$ although the film-cooling-like technique has a higher heat transfer rate.

Conclusions

An experimental investigation was conducted to explore the effects of the size and shape of ribs as well as the presence of secondary air-flow injection on the heat transfer coefficient and pressure drop characteristics of array configurations composed of rectangular individual modules. The experimental results suggest the following conclusions.

(1) The implantation of different sizes and shapes of ribs in the array of rectangular modules is an effective means of heat transfer enhancement. The largest percentage of enhancement occurs at low value of Reynolds number ($Re = 8 \times 10^3$) and increases with increase in the rib's height.

(2) The enhancement in the heat transfer coefficients occurs for all rows downstream of the 5th row of modules with a maximum value of 50% at the row just downstream of the ribs. The rectangular ribs tend to give the best enhancement of the shapes investigated.

(3) The film-cooling-like techniques seems to be an effective means of heat transfer enhancement for electronic modules and has a significant low pressure drop when compared with the results obtained using ribs.

References

Biber, C. R. and Sammakia, B. G. 1986. Transport from discrete heated components in a turbulent channel flow. *Heat Transfer in Electronic Equipment*, **57**, ASME HTD, 1–9

Buller, M. L. and Kilburn, R. F. 1981. Calculation of surface heat transfer coefficients for electronic modules packages. *Heat Transfer in Electronic Equipment*, ASME HTD, **20**, 15–20

Copeland, D. 1992. Effects of channel height and planar spacing on air cooling of electronic components. *Trans. ASME*, **114**, 420–424

Hollworth, B. R. and Durbin, M. 1992. Impingement cooling of electronics. *J. Eng. Heat Transfer*, **114**, 607–613

Kline, S. J. and McClintock, F. A. 1953. Describing uncertainties in single sample experiments. *Mech. Eng.* **75**, 3–8

Lau, S. C., Han, J. C. and Kim, Y. S. 1989. Turbulent heat transfer and friction in pin fin channels with lateral flow ejection. *Trans. ASME*, **111**, 50–58

Lehmann, G. L. and Huang, Y. 1991. Enhanced direct air cooling of electronic components using secondary flow mixing. *Heat Transfer in Electronic Equipment*, ASME HTD, **171**, 11–17

Moffat, R. J., Arvizu, D. E. and Ortega, A. 1985. Cooling electronic components: Forced convection experiment with an air-cooled array. *Heat Transfer In Electronic Equipment*, ASME HTD, **48**, 17–27

Molki, M., Faghri, M. and Ozbay, O. 1994. A new correlation for pressure drop in array of rectangular blocks in air cooled electronic units. *J. Fluids Eng.* **116**, 856–861

Myrum, T. A., Qiu, X. and Acharya, S. 1993. Heat transfer enhancement in a ribbed duct using vortex generators. *Int. J. Heat Mass Transfer*, **36**, 3497–3508

Ratts, E., Amon, C. H., Mikic, B. B. and Patera, A. T. 1988. Cooling enhancement of forced convection air cooled chip array through flow modulation induced vortex shedding cylinders in cross-flow. In *Cooling Technology for Electronic Equipment*, W. Aung (ed.), Hemisphere, Bristol, PA, 183–194

Sparrow, E. M., Niethammer, J. E. and Chaboki, A. 1982. Heat transfer and pressure drop characteristics of array of rectangular modules encountered in electronic equipment. *J. Heat Mass Transfer*, **25**, 961–973

Sparrow, E. M., Vemuri, S. B. and Kadle, D. S. 1983. Enhanced and local heat transfer, pressure drop, and flow visualization for arrays of block-like electronic components. *J. Heat Mass Transfer*, **26**, 689–699

Torikoshi, K., Kawazoe, M. and Kurihara, T. 1988. Convective heat transfer characteristics of arrays of rectangular blocks affixed to one wall of a channel. *Natural and Mixed Convection in Electronic Equipment Cooling*, ASME HTD, **100**, 59–66

Wirtz, R. A. and Dykshoorn, P. 1984. Heat transfer from array of flatpacks in a channel flow. *Proc. 4th Annual Int. Electronics Packaging Society*, Baltimore, MD, 318–326